

Linear Displacement and Straightness Measurement by Fabry-Perot Interferometer Integrated with an Optoelectronic Module

Syuan-Cheng Chang*, Chung-Ping Chang, Yung-Cheng Wang, Ze-Fong You

Abstract: This research develops a three degrees of freedom (DOF) measurement system by integrating Fabry-Perot interferometer and photoelectronic inspection module to determine linear displacement, horizontal and vertical straightness geometric error parameters simultaneously. The interferometer and the photoelectronic inspection module in a three DOF measurement system share the same light source, and the two structures are used to measure linear displacement and straightness errors. The experimental results are utilized to calculate the relevant error parameters according to ISO standards and numerical analysis. They show that after the machine error compensation, the positioning deviation of the system is reduced from 55 μm to 19 μm , corresponding to the reduction of 65%. The accuracy is promoted from 65 μm to 31 μm , about the improvement of 52%. The horizontal and vertical straightness errors of the machine are 4.30 μm and 5.71 μm respectively.

Keywords: interferometer; linear displacement; optoelectronic module; straightness measurement

1 INTRODUCTION

Precision machinery is one of the most important industries in worldwide. And the linear guide is a key component for high precision machine tools and coordinate measuring machines. Due to the deviation in the manufacturing and the assembly of the part, multi-degree-of-freedom geometric errors may occur during the linear motion. The assembly of multiple linear guides also possesses the squareness and the parallelism error. Therefore, the development of a high-precision inspection system is a critical issue. It can be utilized to evaluate the performance of the precision equipment and to be a reference for the subsequent error compensation [1].

The laser interferometric technologies have the advantages of large measuring range, noncontact measurement and high resolution performance. Laser also can trace to the definition of length [2]. Because of those features, Laser interferometers are widely applied to many fields which need high accuracy measurement and calibration [3-5].

The usual commercial interferometer based on a non-common optical path structure is sensitive to environmental disturbances and mechanical vibrations. To eliminate these errors, the proposed Fabry-Perot interferometer system arranged with the common optical path bears the characteristics being more insensitive to such fluctuations. And by the integration of an optoelectronic module, the measurement of the linear displacement and straightness can be achieved.

In order to verify the feasibility of the optimized system, comparison measurements between the proposed Fabry-Perot interferometer and a commercial interferometer have been conducted. According to ISO230-2 norm can reveal that the difference in bidirectional system positioning deviation, repeatability and accuracy. It can prove that the proposed system can be employed for high-precision displacement measurements or the calibration of machine tools.

2 PRINCIPLE AND THEORY

In this chapter, a three degree of freedom (DOF) measurement system has been introduced. The mechanical and an optoelectronic module are integrated into the whole system to measure the linear displacement and straightness error synchronously. This investigation used the He-Ne laser as a light source whose wavelength is 632.8 nm. The signal processing system includes the signal amplification circuit, a low-pass filter circuit and an automatic gain control module. The detail of the fundamental principle and theory reveal as follows.

2.1 Fabry-Perot Interferometer

In this research, the Fabry-Perot interferometer (FPI) serves as the measurement system. FPI is a kind of interferometer with the common path optical structure where the displacement measured is precisely defined by the distance in the optical cavity. For this reason, the effect of the environmental disturbances will be obviously minimized [6] [7].

The amplitude of the transmitted beam can be presented in Eq. (1) to Eq. (4), where A_0 is the amplitude of the incident Laser, R and T are the reflectance and transmittance of the plane mirror, T' is the resultant transmittance of the optical components in the cavity [8], and n is the order number of the transmitted Laser beams.

$$A_1 = A_0 T T'^{1/2} R^0 \quad (1)$$

$$A_2 = A_0 T T'^{3/2} R^1 \quad (2)$$

$$A_3 = A_0 T T'^{5/2} R^2 \quad (3)$$

$$A_n = \frac{\sqrt{2}}{2} A_0 T T'^{(2n-1)/2} R^{n-1} \quad (4)$$

The relevant electric field of the s-type and p-type can be illustrated in Eq. (5) to Eq. (12). In this optical design, δ is

the phase difference of the optical cavity which is $2\pi d/\lambda$, where d is the distance of the optical cavity of FPI

For the electric field of s-type transmitted Laser beams:

$$E_{s1} = \frac{\sqrt{2}}{2} A_0 T T'^{1/2} R^0 \cos(\omega t + kx + \delta) \quad (5)$$

$$E_{s2} = \frac{\sqrt{2}}{2} A_0 T T'^{3/2} R^1 \cos(\omega t + kx + 3\delta) \quad (6)$$

$$E_{s3} = \frac{\sqrt{2}}{2} A_0 T T'^{5/2} R^2 \cos(\omega t + kx + 5\delta) \quad (7)$$

$$E_{sn} = \frac{\sqrt{2}}{2} A_0 T T'^{(2n-1)/2} R^{n-1} \cos[\omega t + kx + (2n-1)\delta] \quad (8)$$

For the electric field of p-type transmitted Laser beams:

$$E_{p1} = \frac{\sqrt{2}}{2} A_0 T T'^{1/2} R^0 \cos(\omega t + kx + \delta + \frac{\pi}{4}) \quad (9)$$

$$E_{p2} = \frac{\sqrt{2}}{2} A_0 T T'^{3/2} R^1 \cos(\omega t + kx + 3\delta + \frac{3\pi}{4}) \quad (10)$$

$$E_{p3} = \frac{\sqrt{2}}{2} A_0 T T'^{5/2} R^2 \cos(\omega t + kx + 5\delta + \frac{5\pi}{4}) \quad (11)$$

$$E_{pn} = \frac{\sqrt{2}}{2} A_0 T T'^{(2n-1)/2} R^{n-1} \cos\left[\omega t + kx + (2n-1)\left(\delta + \frac{\pi}{4}\right)\right] \quad (12)$$

In order to obtain the intensity distribution of the FPI, the summation of the electric field for s-type and p-type are determined by Eq. (13) and Eq. (14).

For the summation of the electric field (s-type):

$$E_s = \frac{\sqrt{2}}{2} A_0 T e^{i(\omega t + kx)} \times \frac{T'^{1/2} e^{i\delta}}{1 - T' R e^{i(2\delta)}} \quad (13)$$

For the summation of the electric field (p-type):

$$E_p = \frac{\sqrt{2}}{2} A_0 T e^{i(\omega t + kx)} \times \frac{T'^{1/2} e^{i\left(\delta + \frac{\pi}{4}\right)}}{1 - T' R e^{i\left(2\delta + \frac{\pi}{2}\right)}} \quad (14)$$

The intensity distribution of s-type and p-type can be denoted by Eq. (15) and Eq. (16).

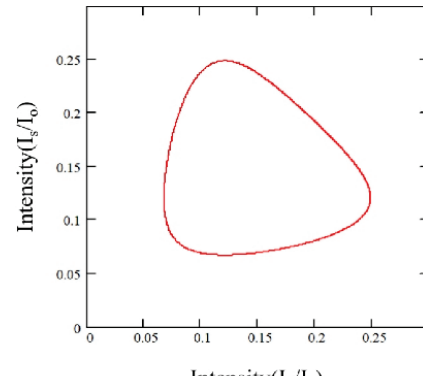
For the intensity of s-type transmitted Laser beams:

$$I_s = E_s \times E_s^* = \frac{\frac{1}{2} A_0^2 T^2 T'}{1 + R^2 T'^2 - 2T' R \cos(2\delta)} \quad (15)$$

For the intensity of p-type transmitted Laser beams:

$$I_p = E_p \times E_p^* = \frac{\frac{1}{2} A_0^2 T^2 T'}{1 + R^2 T'^2 - 2T' R \cos\left(2\delta + \frac{\pi}{2}\right)} \quad (16)$$

The resultant transmittance of the whole optical cavity and the reflectance of the plane mirror are substituted into the equation Eq. (15) and Eq. (16). The simulated intensity distributions are illustrated in Fig. 1.



(a) $R=25\%$, $T=87\%$
Figure 1 Simulation results of signal distribution

2.2 Straightness Measurement

The straightness measurement principle of this system is shown in Fig. 2. This system is combined with a laser light source, a corner cube retroreflector (CCR), a beam splitter (BS) and a 2D-PSD.

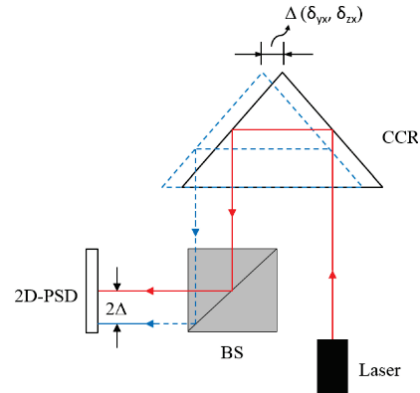


Figure 2 Straightness measurement principle

When the laser beam is incident to the CCR, the beam will be reflected back to the BS, then split to the 2D-PSD which determines the lateral displacement of the laser beam in two directions. For a lateral displacement (δ_{yx} , δ_{zx}) of the CCR, the corresponding offset of the laser spot detected by the 2D-PSD will be 2 times ($2\delta_{yx}$, $2\delta_{zx}$). Therefore, the measurement sensitivity can be enhanced doubly.

The analysis method of straightness error in this research is based on the least square method. And the theoretical equation can be expressed by Eq. (17) to Eq. (19).

$$Y_c = a_0 + a_1 x \quad (17)$$

$$T = \sum_{i=1}^m (y_i - y_{ci})^2 \quad (18)$$

$$T = \sum_{i=1}^m [y_i - (a_0 + a_1 x_i)]^2 \quad (19)$$

When the minimum value of T occurs, its partial differential operation is equal to 0, denoted as Eq. (20) to Eq. (22). Solve the simultaneous equations (Eq. 23, Eq. 24) to obtain a_0 and a_1 , and then substitute them into Eq. (20) to obtain the theoretical equations.

$$dT = \frac{\partial T}{\partial a_0} da_0 + \frac{\partial T}{\partial a_1} da_1 = 0 \quad (20)$$

$$\frac{\partial T}{\partial a_0} = -2 \sum_{i=1}^m (y_i - y_{ci}) = 0 \quad (21)$$

$$\frac{\partial T}{\partial a_1} = -2 \sum_{i=1}^m (y_i - y_{ci}) x_i = 0 \quad (22)$$

$$\sum_{i=1}^m y_{ci} = \sum_{i=1}^m y_i \quad (23)$$

$$\sum_{i=1}^m y_{ci} x_i = \sum_{i=1}^m y_i x_i \quad (24)$$

The straightness error ($E_{\text{straightness}}$) shown in Fig. 3 can be expressed in Eq. (25), where E_{\max} and E_{\min} are the maximum and minimum difference between the measured curve and the fitted line [9].

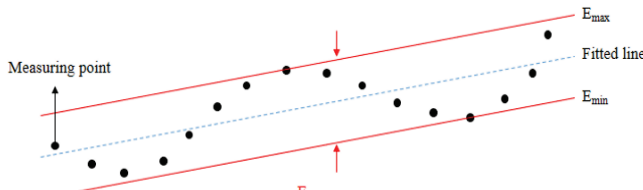


Figure 3 Evaluation of straightness error

$$\sum_{i=1}^m y_{ci} x_i = \sum_{i=1}^m y_i x_i \quad (25)$$

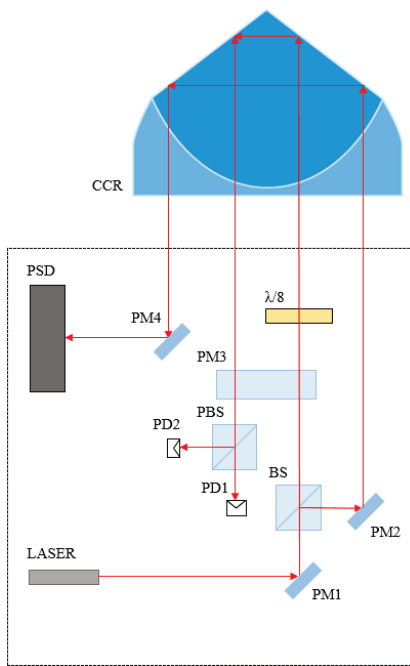


Figure 4 Optomechantronics design of FPI

3 DESIGN OF PROPOSED MEASUREMENT SYSTEM

In this section, the concept and design of this research have been described as follow. The proposed measurement system is based on FPI which is shown in Fig. 4 and Fig. 5. The interferometric signals are received by two Photodiodes (PDs). After the signal amplification processing, the signals will be processed with the high-pass filter circuit to eliminate the DC offset and avoid the signal leakage due to the DC drift.

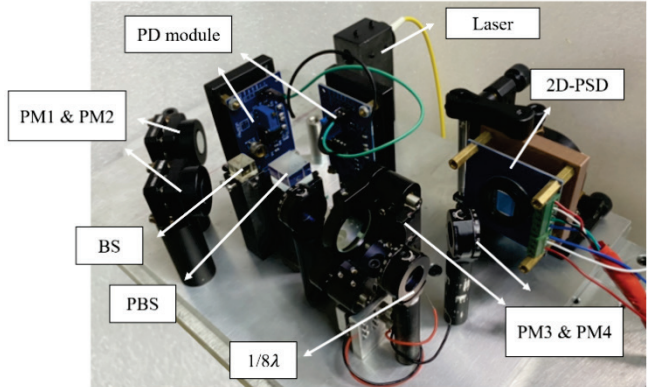


Figure 5 Optical structure of FPI measurement system

4 EXPERIMENTAL RESULTS

In order to verify the ability of the proposed measurement system, a measuring experiment was implemented. The displacement and the straightness error can be measured in this system. And the experimental results are demonstrated as follows.

4.1 Linear Displacement Measurement and Compensation

Fig. 6 is the experimental interference signal of FPI. The reflectance of plane mirrors are about 20%, so the signal pattern is similar to a sinusoid.

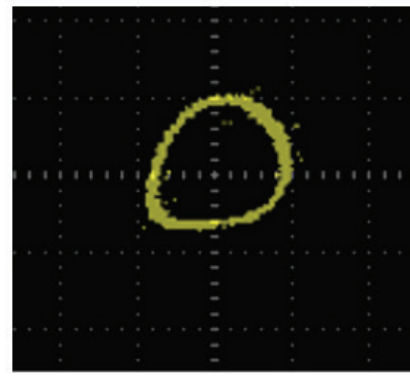


Figure 6 Experimental signal of FPI in X-Y domain

In this experiment, the displacement of linear stage are measured by FPI measurement module, shown in Fig. 7. The measuring range is from 0 to 90 mm with the positioning interval of 10 mm, and each cycle is repeated 5 times. In the comparison experiment, the results with positioning compensation and without compensating are demonstrated as

Figs. 8 to 11. The positioning error of the system is reduced from 55 μm to 19 μm and the accuracy is promoted from 65 μm to 31 μm .

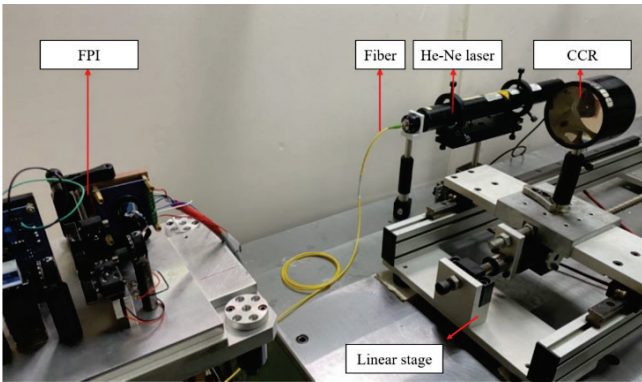


Figure 7 Linear displacement measurement

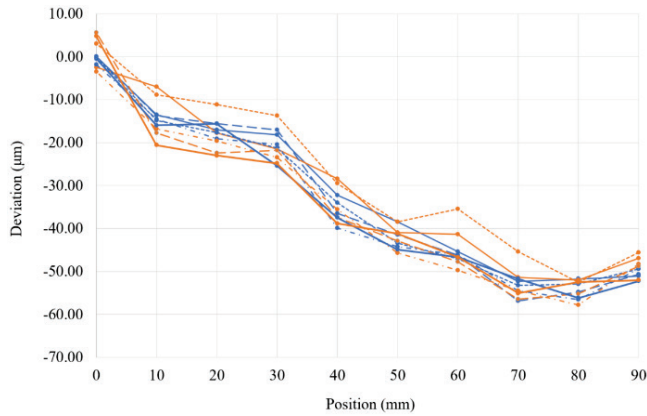


Figure 8 Displacement measurement without compensation

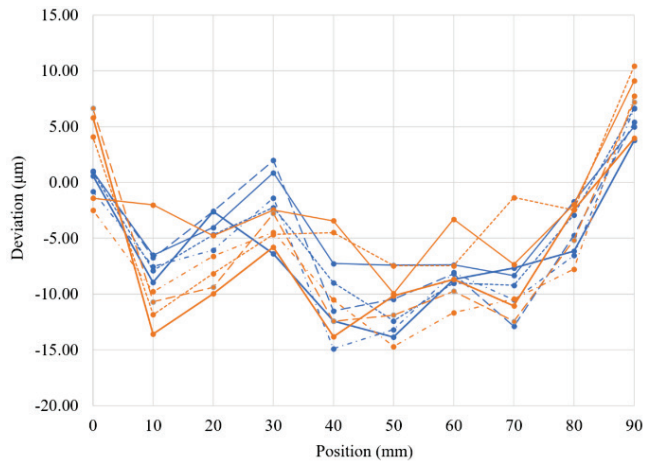


Figure 10 Displacement measurement with compensation

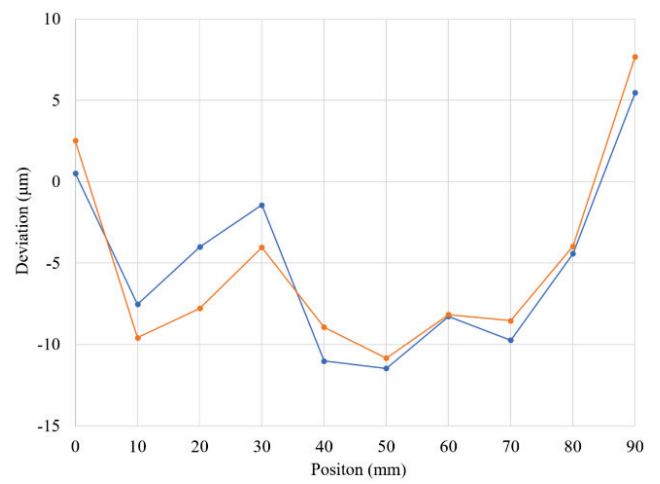


Figure 11 Average displacement deviation with compensation

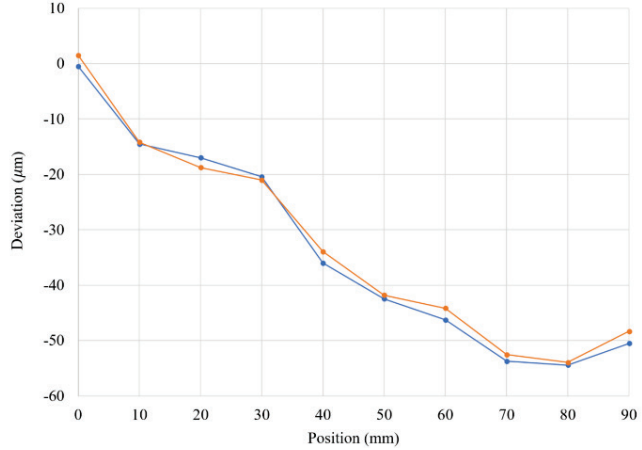


Figure 9 Average displacement deviation without compensation

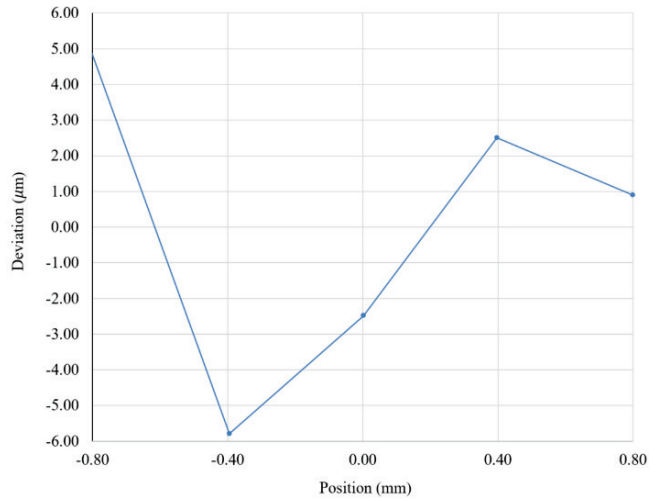


Figure 12 The non-linearity of 2D-PSD in horizontal direction

4.2 Straightness Deviations

In this research, the straightness error can be detected by 2D-PSD, when the linear stage is moving. According to the calibration experiment of 2D-PSD, the non-linearity of 2D-PSD in horizontal and the vertical directions is about -5.78

μm and $5.03 \mu\text{m}$ respectively. The calibration curves are shown in Fig. 12 to Fig. 13.

In the straightness experimental results, the horizontal direction straightness error of linear stage is about $4.30 \mu\text{m}$. The vertical direction straightness error of linear stage is about $5.71 \mu\text{m}$. The results can be shown in Fig. 14 and Fig. 15.

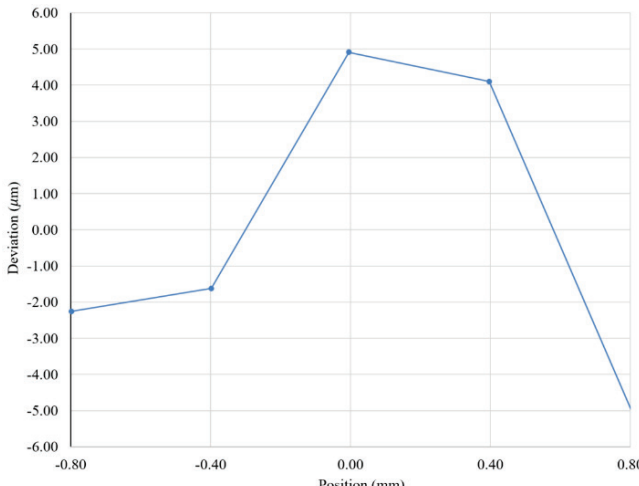


Figure 13 The non-linearity of 2D-PSD in vertical direction

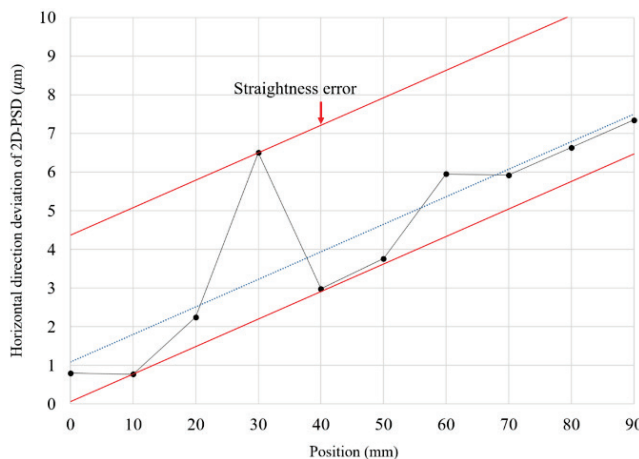


Figure 14 Horizontal direction straightness error of linear stage

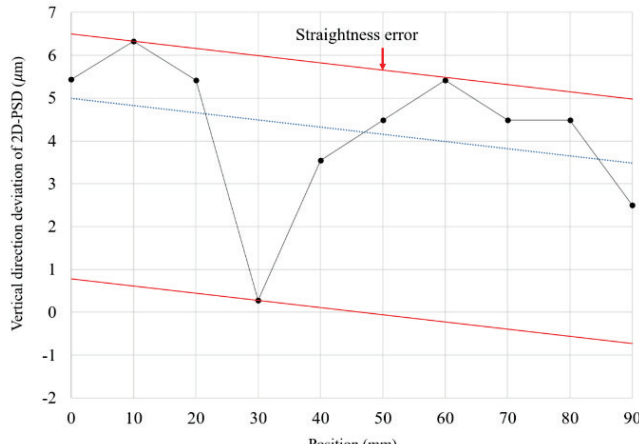


Figure 15 Vertical direction straightness error of movement stage

5 CONCLUSIONS

This article presents a measurement system which can achieve a three degrees of freedom (DOF) measurement by integrating Fabry-Perot interferometer and photoelectronic inspection module to determine linear displacement and straightness errors.

According to the experimental results demonstrated that the positioning deviation of the system is reduced from $55 \mu\text{m}$ to $19 \mu\text{m}$, corresponding to the reduction of 65% . The accuracy is promoted from $65 \mu\text{m}$ to $31 \mu\text{m}$, about the improvement rate of 52% . The horizontal and vertical straightness errors of the stage are $4.30 \mu\text{m}$ and $5.71 \mu\text{m}$ respectively.

Notice

The paper was presented at MOTSP 2022 – 13th International Conference Management of Technology – Step to Sustainable Production, which took place in Primošten/Dalmatia (Croatia) on June 8–10, 2022. The paper will not be published anywhere else.

6 REFERENCES

- [1] Jaeger, G. (2010). Limitations of precision length measurements based on interferometers. *Measurement*, 43, 652-658. <https://doi.org/10.1016/j.measurement.2009.12.030>
- [2] Chang, C.-P., Shih, Y.-C., Chang, S.-C., & Wang, Y.-C. (2019). Laser encoder system for X-Y positioning stage. *Mechatronics*, 63, 102274. <https://doi.org/10.1016/j.mechatronics.2019.102274>
- [3] Xie, F., Li, M., Song, D., Sun, J., & Zhang, T. (2010). Large range and high resolution on-line displacement measurement system by combining double interferometers. *Optics Express*, 18(24). <https://doi.org/10.1364/OE.18.024961>
- [4] Cheng, F. & Fan, K.-C. (2011). High-resolution Angle Measurement based on Michelson Interferometry. *Physics Procedia*, 19, 3-8. <https://doi.org/10.1016/j.phpro.2011.06.118>
- [5] Jeager, G. (2010). Three-Dimensional Nanopositioning and Nanomeasuring Machine with a Resolution of 0.1 nm . *Optoelectronics, Instrumentation and Data Processing*, 46(4), 318-323. <https://doi.org/10.3103/S8756699010040035>
- [6] Lawall, J. R. (2005). Fabry-Perot metrology for displacements up to 50 mm . *Journal of the Optical Society of America A*, 22(12). <https://doi.org/10.1364/JOSAA.22.002786>
- [7] Kong, J., Zhou, A., & Yuan, L. (2017). Temperature insensitive one-dimensional bending vector sensor based on eccentric-core fiber and air cavity Fabry-Perot interferometer. *Journal of Optics*, 19(4). <https://doi.org/10.1088/2040-8986/aa535b>
- [8] Shyu, L. H., Chang, C. P., & Wang, Y. C. (2011). Influence of intensity loss in the cavity of a folded Fabry-Perot interferometer on interferometric signals. *Review of Scientific Instruments*, 82(6), 063103. <https://doi.org/10.1063/1.3596451>
- [9] ISO 230-1:2012. Test code for machine tools – Part 1: Geometric accuracy of machines operating under no-load or quasi-static conditions. *International Standard*.

Authors' contacts:

Syuan-Cheng Chang, PhD student
(Corresponding author)
National Yunlin University of Science and Technology,
123 University Road, Section 3, Doulou, Yunlin 64002, Taiwan, R.O.C.
tso1147279@gmail.com

Yung-Cheng Wang, Prof.
National Yunlin University of Science and Technology,
123 University Road, Section 3, Doulou, Yunlin 64002, Taiwan, R.O.C.
wangyc@untech.edu.tw

Chung-Ping Chang, Assist. Prof.
National Chiayi University,
300 Syuefu Road, Chiayi 600355, Taiwan, R.O.C.
cpchang@mail.ncyu.edu.tw

Ze-Fong You, MS student
National Yunlin University of Science and Technology,
123 University Road, Section 3, Doulou, Yunlin 64002, Taiwan, R.O.C.
M10911029@untech.edu.tw